Magnetic Model Identification of Multi-Three-Phase Synchronous Motors

Magnetic Model Identification of Multi-Three-Phase Synchronous Motors

Sandro Rubino
Dipartimento Energia "G. Ferraris" Politecnico di Torino
10129, Torino, Italy
sandro.rubino@polito.it

Luisa Tolosano
Dipartimento Energia "G. Ferraris" Politecnico di Torino
10129, Torino, Italy
luisa.tolosano@polito.it

Fabio Mandrile
Dipartimento Energia "G. Ferraris" Politecnico di Torino
10129, Torino, Italy
fabio.mandrile@polito.it

Simone Ferrari
Dipartimento Energia "G. Ferraris" Politecnico di Torino
10129, Torino, Italy
simone.ferrari@polito.it

Eric Armando
Dipartimento Energia "G. Ferraris" Politecnico di Torino
10129, Torino, Italy
eric.armando@polito.it

Radu Bojoi
Dipartimento Energia "G. Ferraris" Politecnico di Torino
10129, Torino, Italy
radu.bojoi@polito.it

***Abstract*—Multi-three-phase motor drives are experiencing a significant development among the multiphase solutions since they are configured as multiple three-phase units operating in parallel. Although the literature reports several torque controllers able to deal with multi-three-phase motors, most of them obtain high performance of torque regulation as long as flux and torque maps of the machine are known. The literature currently reports very few contributions dealing with the experimental identification of flux and torque maps of multi-three-phase synchronous motors operating in healthy and open-three-phase fault conditions. In addition, almost all these research contributions focus on dual-three-phase machines. This paper thus proposes an experimental test procedure to directly identify the flux and torque maps of a multi-three-phase synchronous motor featuring an arbitrary number of three-phase winding sets. The proposed identification procedure also allows an accurate machine analysis considering all potential open-three-phase fault scenarios. Experimental results obtained on a 12-phase interior permanent magnet synchronous motor using a quadruple-three-phase configuration of the stator winding are presented. Besides, flux and torque maps obtained in severe open-three-phase fault conditions are shown, fully validating the proposed identification procedure.**

Keywords—magnetic model identification, multiphase motors, parameters identification, synchronous motors.

I. Introduction

The current electrification processes involving transport are leading to the development of several solutions, including multi-three-phase motor drives [1]–[3]. Indeed, these multiphase systems are receiving significant interest from the industry since they allow three-phase modularity of both the electric motor and the power electronics converter feeding it [4]–[6]. Considering the electric motor, the stator consists of independent three-phase winding sets with isolated neutral points, simplifying the design procedures. Considering the power electronics converter, a three-phase inverter typically feeds each three-phase winding set, allowing the use of the three-phase technologies [7]–[9] and thus reducing costs and development time. A schematic view of a multi-three-phase drive is shown in Fig. 1 to help the understanding.

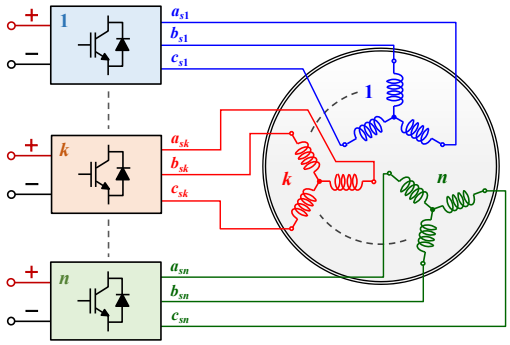

Fig. 1. View of a multi-three-phase drive topology.

Together with the previously mentioned pros, multi-three-phase drives also allow for extending the three-phase modularity to the fault tolerance [1], [4]. Indeed, in the case of an open-phase fault involving one unit (winding set plus inverter feeding it), this is just disconnected from the dc supply, allowing a post-fault operation without low-order harmonics on the dc-link currents [2].

Considering multi-three-phase synchronous machines, the literature currently reports different torque controllers dealing with them, including solutions able to perform current or torque-sharing strategies among the three-phase units [4]–[6]. However, almost all these control solutions require the knowledge of the machine magnetic model, i.e., the current-to-flux and current-to-torque maps. This way, high performance of torque regulation is achieved in terms of accuracy, dynamic response, and efficiency.

Currently, very few research contributions dealing with the experimental identification of flux and torque maps of multi-three-phase synchronous motors are reported in the literature. Moreover, most of them are focused on dual-three-phase solutions [10], [11], i.e., 6-phase motors adopting stator winding configurations that are typically symmetrical or asymmetrical, i.e., featuring a specific displacement angle between the magnetic axes of two namesake phases of two adjacent three-phase winding sets [12]. For instance, the displacement angle is

30 degrees for an asymmetrical dual-three-phase motor, while 60 degrees for a symmetrical dual-three-phase one [12], [13].

Compared to state-of-the-art, this paper proposes an experimental procedure that directly identifies flux and torque maps of multi-three-phase synchronous motors operating in normal and severe fault conditions, i.e., loss of one or more three-phase winding sets. The contributions brought by this paper to the existing literature are summarized as follows.

- The identification procedure can be implemented on any multi-three-phase synchronous motor, regardless of *i*) the number of three-phase winding sets, *ii*) the rotor structure that can present anisotropy or permanent magnets (PMs), or both, and *iii*) the configuration of the stator winding that can also be different from the conventional symmetrical or asymmetrical ones.
- There is no need for a multi-three-phase sinusoidal supply to perform the proposed identification procedure as the target inverter of the motor under test (MUT) is used.
- A calibrated data recorder is used to directly measure the pulse-width modulation (PWM) waveforms of line-to-line voltages and phase currents of each three-phase winding set. This way, the output results of the test procedure may be certified if required since there is no need to estimate and compensate for the voltage errors introduced by the inverter units [14].
- Flux and torque maps in open-three-phase fault conditions are obtained by simply turning off one or more three-phase inverter units during the execution of the identification procedure, thus testing the faulty configuration of interest straightforwardly.

The proposed test procedure has been implemented to identify flux and torque maps of a 12-phase PM-assisted synchronous reluctance (PM-SyR) motor adopting a quadruple three-phase configuration of the stator winding, rated 60 kW @ 1000 r/min. The paper is organized as follows. Section II reports the theoretical background behind the proposed identification procedure, while Section III describes the latter in detail. Section IV shows the experimental results providing validation of the proposed identification method. Finally, Section V reports the paper's conclusion.

II. Theoretical Background

According to the literature, several modelling approaches can be used to model a multi-three-phase motor, like the vector space decomposition (VSD) [15], multi-stator (MS) [1], [16], or the more recent adaptive decoupled MS (A-DMS) [17]. Although any of these approaches can properly model a multi-three-phase machine, the proposed identification procedure uses the A-DMS modeling.

The A-DMS approach decomposes the machine model into common- and differential- mode subspaces [17]–[19]. Assuming a sinusoidal distribution of the stator windings, magnetizing flux and torque are produced in the common-mode subspace. The differential-mode subspaces map instead the unbalances between the winding sets in terms of currents, flux, and voltages. The A-DMS model is computed using the modular matrix transformation reported in [17], whose dimension depends on the number of healthy three-phase winding sets.

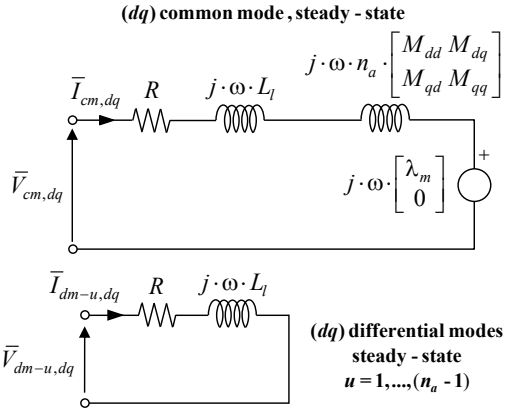

Fig. 2. Equivalent A-DMS circuit of a multi-three-phase synchronous motor.

The advantages of the A-DMS modeling are evident since it is possible to overcome the VSD limitations [13] in terms of stator winding configurations that can be different from the regular ones, i.e., symmetrical or asymmetrical. In addition, compared to MS modeling, the A-DMS allows for removing the magnetic coupling between the three-phase winding sets but keeping modularity [17], [18]. Finally, because the A-DMS considers only the healthy winding sets of the machine, the differential-mode currents can still be zero after an open-three-phase fault event. Indeed, although this condition is valid only if the healthy winding sets operate balanced with each other, it corresponds to the MUT operation when performing the proposed identification procedure, thus all the more so justifying the adoption of the A-DMS modeling.

According to the above considerations, the common-mode equations of the MUT are considered, corresponding to those of a three-phase synchronous motor [20], [21]. Therefore, the following *dq* equations rule the common-mode variables, from which the steady-state equivalent circuit of Fig. 2 is obtained.

$$\begin{cases} \bar{v}_{cm,dq} = R\cdot\bar{i}_{cm,dq} + \dfrac{d}{dt}\bar{\lambda}_{cm,dq} + j\cdot\omega\cdot\bar{\lambda}_{cm,dq} \\ \bar{\lambda}_{cm,dq} = L_l\cdot\bar{i}_{cm,dq} + n_a\cdot\begin{bmatrix}M_{dd} & M_{dq}\\ M_{qd} & M_{qq}\end{bmatrix}\cdot\bar{i}_{cm,dq} + \begin{bmatrix}\lambda_m\\ 0\end{bmatrix} \end{cases} \quad (1)$$

In (1), $\bar{z}_{cm,dq}=[z_{cm,d}\ z_{cm,q}]^t$ is a generic common-mode stator vector expressed in rotating *dq* coordinates; ω is the rotor electric speed computed as pole pair *p* times the mechanical one ω_m; *v*, *i*, and λ have the meaning of voltage, current, and flux linkage, respectively, reported as uppercase in Fig. 2 to denote steady-state variables; *R* is the stator resistance; λ_m is the fundamental component of the PM flux linkage, equal to zero for motors without PMs like SyR ones; L_l is the stator leakage inductance, M_{dd} and M_{qq} are the self-magnetizing *dq* inductances while M_{dq} and M_{qd} are the cross-magnetizing ones; n_a is the number of healthy winding sets, this less or at most equal to that rated number of MUT's winding sets *n*; *j* is the complex operator in matrix form. According to Fig. 2, $\bar{z}_{dm-u,dq}=[z_{dm\text{-}u,d}\ z_{dm\text{-}u,q}]^t$ is a generic differential-mode stator vector expressed in rotating *dq* coordinates.

It is highlighted in (2) that the common-mode *dq* variables are computed by averaging the corresponding stator *dq* vectors belonging to healthy winding sets $\bar{z}_{k,dq}=[z_{k,d}\ z_{k,q}]^t$ ($k = 1,\ldots,n_a$).

$$\bar{z}_{cm,dq} = \frac{1}{n_a} \cdot \sum_{k=1}^{n_a} \bar{z}_{k,dq} \tag{2}$$

The electromagnetic torque is computed according to (3) as the outer product between the common-mode stator vectors of flux linkage and current and considering the number of healthy winding sets [17].

$$T_e = (3/2) \cdot n_a \cdot p \cdot \left(\lambda_{cm,d} \cdot i_{cm,q} - \lambda_{cm,q} \cdot i_{cm,d} \right) \tag{3}$$

The proposed identification procedure exploits the steady-state solutions of the common-mode model (1). According to Fig. 2, the steady-state common-mode equations of the machine are thus computed as follows.

$$\begin{cases} V_{cm,d} = R \cdot I_{cm,d} - \omega \cdot \Lambda_{cm,q} \\ V_{cm,q} = R \cdot I_{cm,q} + \omega \cdot \Lambda_{cm,d} \\ \Lambda_{cm,d} = \left(L_l + n_a \cdot M_{dd} \right) \cdot I_{cm,d} + n_a \cdot M_{dq} \cdot I_{cm,q} + \lambda_m \\ \Lambda_{cm,q} = n_a \cdot M_{qd} \cdot I_{cm,d} + \left(L_l + n_a \cdot M_{qq} \right) \cdot I_{cm,q} \end{cases} \tag{4}$$

Also, the following properties characterizing the magnetizing *dq* inductances of synchronous motors are considered [21].

$$\begin{cases} M_{dd}\left(i_{cm,d}, i_{cm,q} \right) = M_{dd}\left(i_{cm,d}, \left| i_{cm,q} \right| \right) \\ M_{dq}\left(i_{cm,d}, i_{cm,q} \right) = M_{dq}\left(i_{cm,d}, \left| i_{cm,q} \right| \right) \cdot sign\left(i_{cm,q} \right) \\ M_{qd}\left(i_{cm,d}, i_{cm,q} \right) = M_{qd}\left(i_{cm,d}, \left| i_{cm,q} \right| \right) \cdot sign\left(i_{cm,q} \right) \\ M_{qq}\left(i_{cm,d}, i_{cm,q} \right) = M_{qq}\left(i_{cm,d}, \left| i_{cm,q} \right| \right) \end{cases} \tag{5}$$

Let's consider the MUT operating at constant positive speed $\omega^* > 0$ with positive common-mode *dq* currents, i.e., $i_{cm,d} = I_{cm,d}^* > 0$ and $i_{cm,q} = I_{cm,q}^* > 0$. According to (4), the steady-state *dq* components of the common-mode voltage vector, specially denoted with superscript ^{P}, are computed as:

$$\begin{cases} V_{cm,d}^P = R \cdot I_{cm,d}^* - \omega^* \cdot \Lambda_{cm,q}^* \\ V_{cm,q}^P = R \cdot I_{cm,q}^* + \omega^* \cdot \Lambda_{cm,d}^* \end{cases} \tag{6}$$

where $\Lambda_{cm,d}^*$ and $\Lambda_{cm,q}^*$ are the *dq* components of the common-mode flux linkage vector for the considered combination of common-mode *dq* currents. Let's now consider reversing the common-mode *q*-axis current component, i.e., $i_{cm,d} = I_{cm,d}^* > 0$ and $i_{cm,q} = -I_{cm,q}^* < 0$. According to (5), the steady-state *dq* components of the common-mode voltage vector, now specially denoted with superscript ^{N}, are computed from (4) as:

$$\begin{cases} V_{cm,d}^N = R \cdot I_{cm,d}^* + \omega^* \cdot \Lambda_{cm,q}^* \\ V_{cm,q}^N = -R \cdot I_{cm,q}^* + \omega^* \cdot \Lambda_{cm,d}^* \end{cases} \tag{7}$$

It is noted that the *dq* components of the common-mode flux linkage vector $\Lambda_{cm,d}^*$ and $\Lambda_{cm,q}^*$ corresponding to an arbitrary combination of common-mode *dq* currents $i_{cm,d} = I_{cm,d}^*$ and $i_{cm,q} = I_{cm,q}^*$ can be easily computed by combining the *dq* common-mode voltages from the conditions (6), (7) as in (8).

$$\begin{cases} \Lambda_{cm,d}^* = \dfrac{V_{cm,q}^P + V_{cm,q}^N}{2 \cdot \omega^*} \quad , \quad \Lambda_{cm,q}^* = \dfrac{V_{cm,d}^N - V_{cm,d}^P}{2 \cdot \omega^*} \end{cases} \tag{8}$$

This way, the voltage drops on the stator resistance are compensated, making it unnecessary to account for them in evaluating the *dq* components of the common-mode flux linkage vector [22]. Finally, let's assume a balanced operation of the healthy three-phase winding sets. In this case, the common-mode *dq* components of flux linkage vector correspond to the actual ones of each healthy winding set according to (2), (9).

$$\begin{cases} \{ i_{k,d} = i_{cm,d} \ , \ i_{k,q} = i_{cm,q} \quad \forall k = 1,...,n_a \ \Rightarrow \\ \Rightarrow \begin{cases} \lambda_{k,d}\left(i_{k,d}, i_{k,q} \right) = \lambda_{cm,d}\left(i_{cm,d}, i_{cm,q} \right) \\ \lambda_{k,q}\left(i_{k,d}, i_{k,q} \right) = \lambda_{cm,q}\left(i_{cm,d}, i_{cm,q} \right) \end{cases} \quad \forall k = 1,...,n_a \end{cases} \tag{9}$$

Thanks to the A-DMS modeling, the flux maps of the common-mode subspace are thus representative of each three-phase winding set in the case of a balanced operation between them. Also, according to (3), (10), the torque map of each three-phase winding set is obtained from that of the common-mode subspace by simply scaling it by the number of healthy winding sets.

$$\begin{aligned} &\{ i_{k,d} = i_{cm,d} \ , \ i_{k,q} = i_{cm,q} \quad \forall k = 1,...,n_a \ \Rightarrow \\ &\Rightarrow T_k\left(i_{k,d}, i_{k,q} \right) = (3/2) \cdot p \cdot \left(\lambda_{k,d} \cdot i_{k,q} - \lambda_{k,q} \cdot i_{k,d} \right) = \\ &\qquad = (1/n_a) \cdot T_e\left(i_{cm,d}, i_{cm,q} \right) \quad \forall k = 1,...,n_a \end{aligned} \tag{10}$$

In summary, identifying flux and torque maps of each three-phase winding set of a multi-three-phase synchronous motor can be performed by simply considering flux and torque maps of the common-mode subspace obtained from the A-DMS modeling subject to considering the three-phase units operate balanced each other.

III. Identification Procedure

The proposed identification procedure needs a standard rig for testing multi-three-phase motor drives. The measurement and test setup for a generic three-phase winding set k ($k = 1,\ldots,n$) of the MUT is shown in Fig. 3 to aid the understanding.

A. Experimental setup

The MUT speed is set by a speed-controlled driving machine (DM) acting as a prime mover. Although not mandatory, a torque transducer can be mounted between MUT and DM, thus measuring the MUT torque T_m and getting further results validating the proposed identification procedure. The mechanical position of the MUT ϑ_m is instead measured using a position sensor like an encoder or resolver or, if available, the position feedback provided by the torque transducer.

According to Fig. 3, each three-phase winding set k ($k = 1,\ldots,n$) is fed by a three-phase inverter unit receiving the duty-cycles commands by the digital controller implementing the proposed identification procedure. Each three-phase inverter unit, in turn, must be supplied by a bidirectional dc source that can be shared with the other inverter units for simplicity. Therefore, flux and torque maps of the MUT in open-three-phase fault conditions are obtained by turning OFF one or more three-phase inverter units according to the faulty configuration of interest and executing the proposed test procedure afterwards.

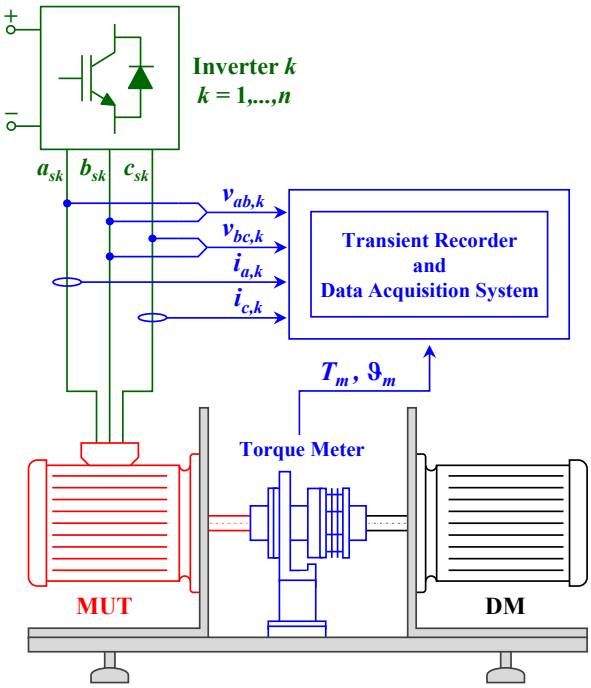

Fig. 3. Test and measurement setup for one three-phase unit of the MUT.

Regarding the measurement setup, two arbitrary line-to-line voltages, e.g., $v_{ab,k}$ and $v_{bc,k}$, and two arbitrary phase currents, e.g., $i_{a,k}$ and $i_{c,k}$, are measured for each three-phase winding set k (k = 1,…,n). Because the MUT is fed by PWM inverter units, the MUT waveforms of voltages and currents must be measured using high-bandwidth calibrated sensors. For instance, shielded cables connected to high-voltage and high-resolution cards for sensing the line-to-line voltages, while closed-loop Hall effect transducers for sensing the phase currents. Finally, a calibrated high-sample rate data recorder collects electric and mechanical measurements and elaborates them post-processing (see Fig. 3).

B. Test procedure

The MUT speed is set at a constant value ω_m^*, guaranteeing a proper amplitude of the machine's back-electromotive force (back-emf) and negligible iron losses simultaneously. Typically, a speed between one-fifth to one-third of the rated value is chosen [22]. An A-DMS-based current vector control (CVC) scheme is implemented in the digital controller to inject a common-mode stator current vector having predefined dq components. In parallel, the differential-mode currents should be controlled at zero to operate the healthy winding sets balanced with each other. This way, the dq components of the stator current vector correspond to the actual dq currents of each three-phase winding set. At the same time, flux and torque maps of each three-phase winding set are easily obtained from those of the common-mode subspace according to (9), (10).

The block diagram of the A-DMS-based CVC scheme is shown in Fig. 4, where the superscript * denotes a reference variable. According to the A-DMS approach, the matrix transformation $[T_D]$ computing common- and differential- mode currents in stationary coordinates αβ from those in k-set phase coordinates abc_k (k=1,…,n_a) is applied only to the healthy winding sets and whose definition is provided in [17].

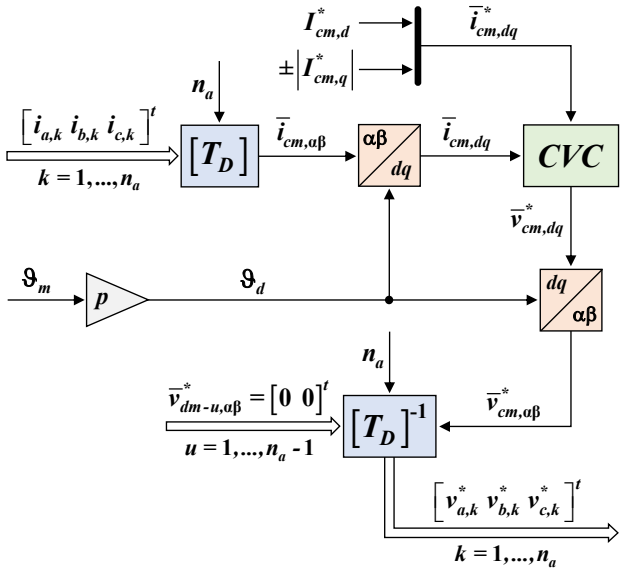

Fig. 4. Block diagram of the A-DMS-based CVC scheme.

Instead, the inverse matrix transformation $[T_D]^{-1}$ is applied to the common- and differential- mode reference voltages in stationary coordinates αβ to compute their corresponding values in k-set phase coordinates abc_k (k=1,…,n_a) only for healthy inverter units. Regarding the control of the differential-mode currents, it may be possible to simplify the A-DMS-based CVC scheme by directly setting the differential mode reference voltages at zero, as shown in Fig. 4. However, this simplification is suggested if the MUT does not present significant asymmetries between the winding sets in terms of resistance or leakage inductance, or both.

According to Section II, for each dq combination ($I_{cm,d}^*$, $I_{cm,q}^*$) of the common-mode stator current vector, the MUT is sequentially operated with positive ($+|I_{cm,q}^*|$) and negative ($-|I_{cm,q}^*|$) values of the q-axis current component. This way, the resistive voltage drops are ruled out from evaluating the dq components of the flux linkage vector, as demonstrated in (8). In other words, once a positive or negative common-mode q-axis current is imposed, and the stator currents are settled, the steady-state PWM waveforms of phase currents and line-to-line voltages of each winding set (see Fig. 3) are sampled and stored by the data recorder. This way, the time-fundamental active P_k and reactive Q_k powers of each healthy three-phase winding set k (k=1,…,n_a) can be computed as post-processing of the acquired data. Subsequently, the steady-state dq components of the common-mode voltage vector when injecting a positive common-mode q-axis current can be computed using (11) if the differential-mode currents are kept null.

$$\begin{cases} V_{cm,d}^P = \dfrac{2}{3 \cdot n_a \cdot I_{cm}^{*\,2}} \cdot \left(I_{cm,d}^* \cdot \sum_{k=1}^{n_a} P_k - \left| I_{cm,q}^* \right| \cdot \sum_{k=1}^{n_a} Q_k \right) \\ V_{cm,q}^P = \dfrac{2}{3 \cdot n_a \cdot I_{cm}^{*\,2}} \cdot \left(\left| I_{cm,q}^* \right| \cdot \sum_{k=1}^{n_a} P_k + I_{cm,d}^* \cdot \sum_{k=1}^{n_a} Q_k \right) \end{cases} \tag{11}$$

where:

$$I_{cm}^{*\,2} = I_{cm,d}^* \cdot I_{cm,d}^* + I_{cm,q}^* \cdot I_{cm,q}^* \tag{12}$$

Similarly, the steady-state *dq* components of the common-mode voltage vector when injecting a negative common-mode *q*-axis current are computed using (13).

$$\begin{cases} V_{cm,d}^{N} = \dfrac{2}{3 \cdot n_a \cdot I_{cm}^{*\,2}} \cdot \left(I_{cm,d}^{*} \cdot \sum_{k=1}^{n_a} P_k + \left| I_{cm,q}^{*} \right| \cdot \sum_{k=1}^{n_a} Q_k \right) \\ V_{cm,q}^{N} = \dfrac{2}{3 \cdot n_a \cdot I_{cm}^{*\,2}} \cdot \left(-\left| I_{cm,q}^{*} \right| \cdot \sum_{k=1}^{n_a} P_k + I_{cm,d}^{*} \cdot \sum_{k=1}^{n_a} Q_k \right) \end{cases} \quad (13)$$

Therefore, for each *dq* combination ($I_{cm,d}^{*}$, $I_{cm,q}^{*}$) of the common-mode stator current vector, the steady-state *dq* components of the common-mode voltage vector corresponding to positive- (6) and negative- (7) common-mode *q*-axis current are obtained using (11) and (13), respectively. This way, the *dq* components of the common-mode flux linkage vector ($\Lambda_{cm,d}^{*}$, $\Lambda_{cm,q}^{*}$), corresponding to a specific *dq* combination ($I_{cm,d}^{*}$, $I_{cm,q}^{*}$) of the common-mode stator current vector, are straightforwardly computed using (8) where $\omega^{*} = p \cdot \omega_m^{*}$.

The proposed identification procedure is organized to test several *dq* combinations of the common-mode stator current vector according to a polar mesh grid whose limit corresponds to the maximum value of the MUT phase currents. In addition, as for the three-phase synchronous motors, only positive target values of the common-mode *q*-axis current $I_{cm,q}^{*}$ should be tested thanks to the symmetries of the flux maps [22], i.e., (5). For SyR motors, even only positive target values of the common-mode *d*-axis current $I_{cm,d}^{*}$ should be tested since the flux maps are symmetric along both *dq* axes [20], [23], [24]. Finally, once all *dq* combinations of the common-mode stator current vector are tested, the common-mode flux $\lambda_{cm,d}(i_{cm,d},i_{cm,q})$, $\lambda_{cm,q}(i_{cm,d},i_{cm,q})$ and torque $T_e(i_{cm,d},i_{cm,q})$ maps of the MUT are obtained.

Regardless of the MUT (with or without PMs), a proper cooling time should be implemented between testing one *dq* combination and the subsequent one. For PM synchronous motors, this action is instead mandatory to keep the PMs temperature constant and close to that of the external ambient, unaltering the flux maps along the *d*-axis [25]. Conversely, if flux and torque maps of the MUT must be evaluated in rated thermal conditions, then a temperature-controlled method like the one proposed in [25] for three-phase synchronous motors may be adopted.

IV. Experimental Validation

The machine used for the experimental validation is a 4-pole, 12-phase PM-SyR adopting an asymmetrical quadruple three-phase stator winding configuration (full-pitch windings with one slot/pole/phase), as schematically shown in Fig. 5. The rated power of the MUT is 60 kW @ 1000 r/min while the other primary rated data are listed in Table I.

A. Test rig

According to Section III-A (see Fig. 3), the MUT speed has been set using a speed-controlled DM acting as a prime mover. Besides, the torque transducer T40B from HBK GmbH has been mounted along the mechanical coupling between MUT and DM, further validating the proposed identification procedure results, as shown in Fig. 6. The rotor mechanical position has been measured using the incremental encoder embedded with the MUT, having a resolution of 1024 pulses/rev.

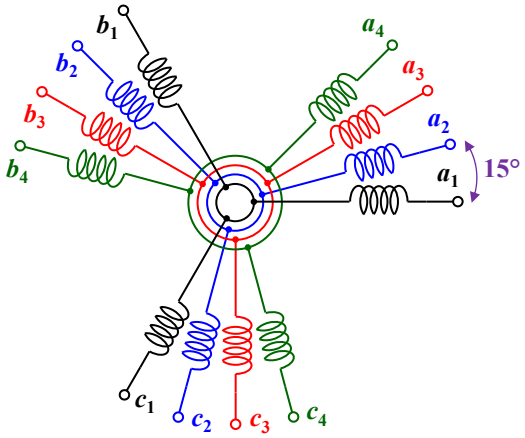

Fig. 5. View of a 12-phase winding adopting an asymmetrical quadruple-three-phase configuration.

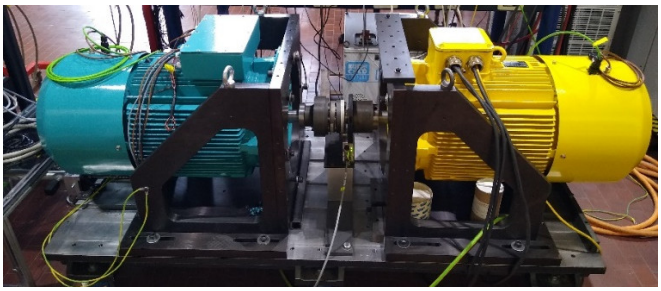

Fig. 6. View of the MUT (left, blue motor), torque transducer HBK T40B (middle), and DM (right, yellow motor).

TABLE I. Machine Primary Data

Phase number	12 (4·3-phase)
Pole number	4
Rated power	60 kW
Rated speed	1000 r/min
Rated phase voltage	245 V (RMS)
Rated phase current	21.25 A (RMS)

The power converter consists of four independent three-phase inverter units (1200 V – 100 A), fed at 600 V by a common bidirectional dc source, with software implemented dead-time of 1.5 µs [26]. The digital controller is the prototyping board dSPACE DS1103 while the identification procedure has been developed in C code. Switching and sampling frequencies have been set at 5 kHz to emulate a typical scenario of industrial implementations.

According to the measurement setup shown in Fig. 3, line-to-line voltages and phase currents have been measured for each three-phase winding set. In detail, the PWM line-to-line voltages have been sensed using shielded cables connected to the high-voltage and high-resolution voltage cards GN610B from HBM Gmbh. In parallel, the PWM phase currents have been measured using the high-bandwidth closed-loop transducers IT200-S Ultrastab from LEM. Finally, all measurements have been sampled and stored using the calibrated transient recorder and data acquisition system GEN7tA from HBM GmbH, adopting a sampling frequency of up to 2 MS/s.

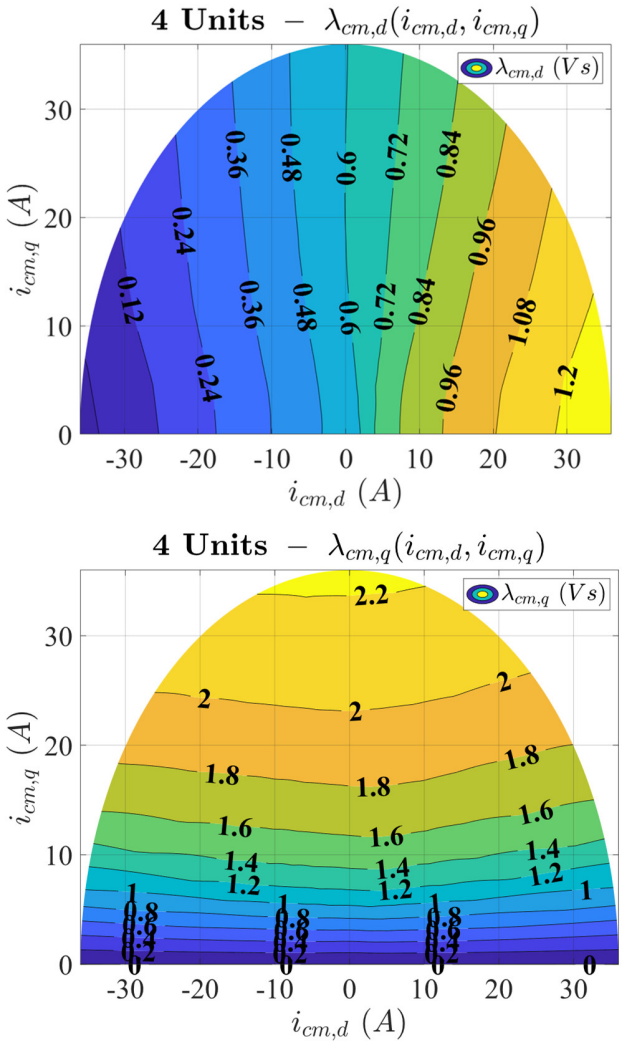

Fig. 7. Common-mode flux maps with four three-phase units ON.

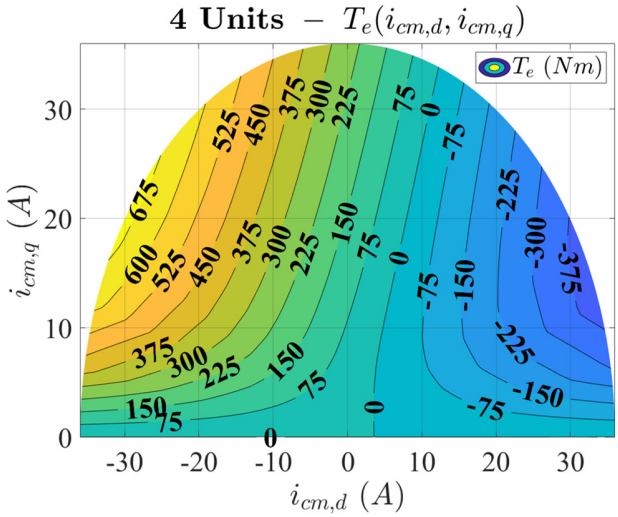

Fig. 8. Common-mode torque map with four three-phase units ON.

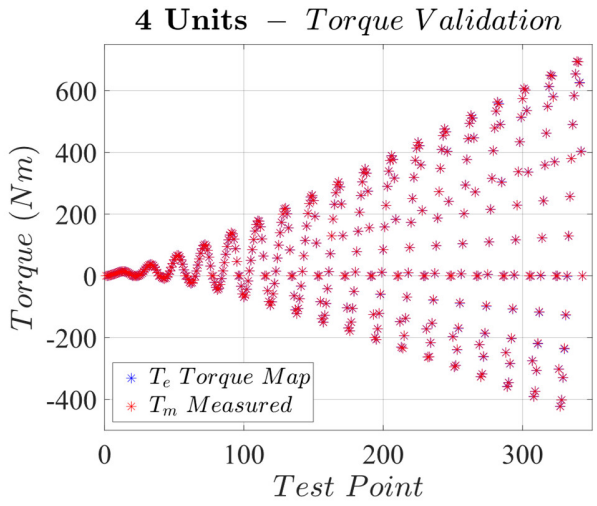

Fig. 9. Comparison between torque map with four three-phase units ON and corresponding measured values using the torque transducer T40B.

B. Experimental results

The MUT speed has been set at 250 r/min using the DM, i.e., a fourth of the rated speed (see Table I). Using the A-DMS-based CVC scheme shown in Fig. 4, the amplitude of the common-mode current vector I_{cm}^* has been set in the range 0 – 36 A with a step of 2 A, thus corresponding to a MUT overload of about 120 % (see Table I). In parallel, the position of the common-mode current vector γ^* to the *d*-axis has been set in the range of 0 – 180 degrees with a step of 10 degrees, mapping the *dq* plane completely.

The MUT operation in healthy conditions has been considered first, i.e., operating all three-phase units. Using the procedure described in Section III-B, the common-mode flux and torque maps shown in Figs. 7 – 8 have been obtained. It is noted how they consist of the typical flux and torque maps of a PM-SyR motor in which most of the torque is produced by magnetic anisotropy [27]. Besides, most of the magnetizing flux is produced along the *q*-axis since the MUT rotor exhibits four flux barriers along the *d*-axis. According to Section II, the common-mode flux maps correspond to those of each winding set if considering a balanced operation among them.

By rescaling the common-mode torque map by the number of active units, i.e., 4 in this case, the torque map of each three-phase set considering a balanced operation among them is instead obtained. The comparison between the torque computed from the flux maps and the measured torque using the transducer for each test point of the identification procedure is shown in Fig. 9. It is noted how these values perfectly match each other in each test point, validating the proposed identification procedure results. Instead, Fig. 10 shows the profile of the PM flux linkage while executing the identification procedure. This profile has been obtained by measuring the MUT's back-emf while waiting for the cooling time between one test point and the subsequent one. It is noted how the PM flux linkage did not change significantly (about 1 %), confirming that the flux and torque maps have been identified by keeping the PMs at a constant temperature equal to that of the external ambient.

The MUT has been subsequently identified in severe open-three-phase fault conditions, turning OFF the three-phase units 2 and 4.

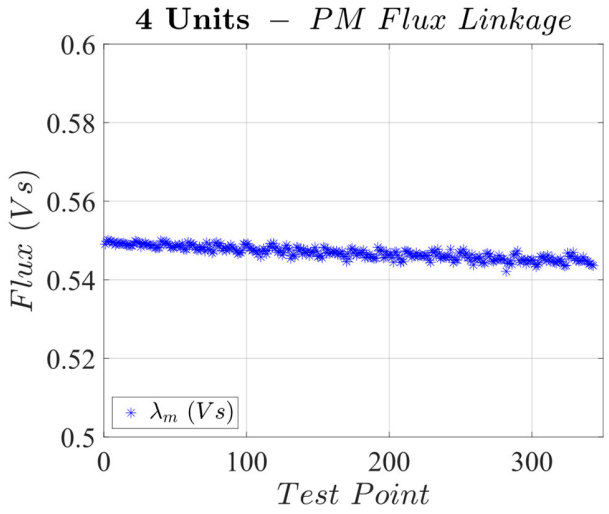

Fig. 10. PM flux linkage while executing the identification procedure.

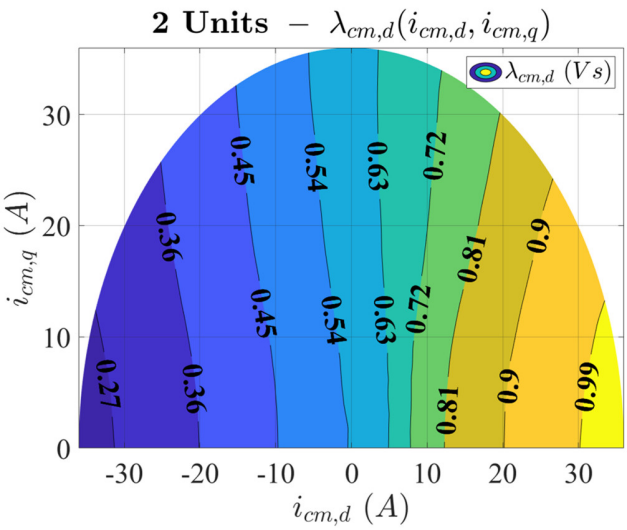

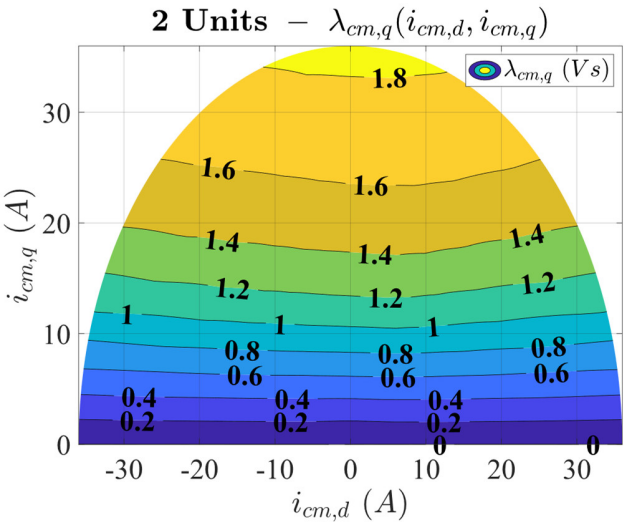

Fig. 11. Common-mode flux maps with two three-phase units ON.

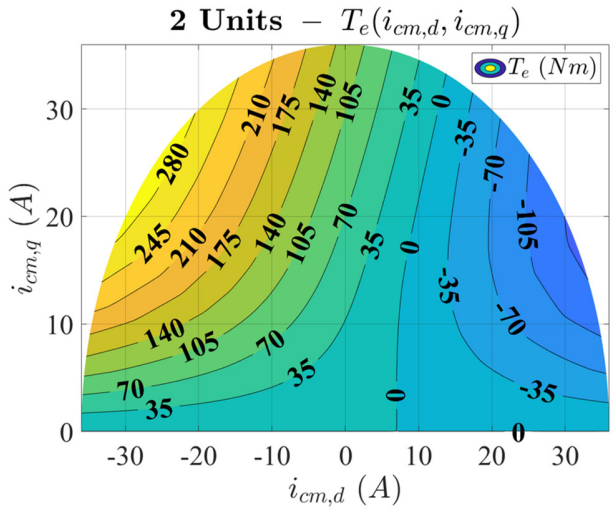

Fig. 12. Common-mode torque map with two three-phase units ON.

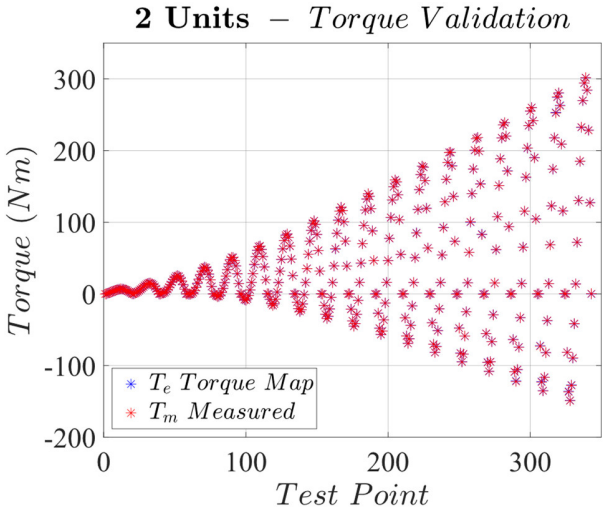

Fig. 13. Comparison between torque map with two three-phase units ON and corresponding measured values using the torque transducer T40B.

Therefore, the machine has been operated as an equivalent asymmetrical dual-three-phase PM-SyR in these conditions [10]. The common-mode flux and torque maps obtained in these conditions are shown in Figs. 11 – 12. The significant derating of the MUT performance in these fault conditions is noted. Indeed, the maximum torque produced by the MUT by injecting the maximum current of 36 A in the healthy winding sets significantly decreases from about 693 Nm to 301 Nm. This result is expected and confirms how the multi-three-phase synchronous motors guarantee torque capability after an open-three-phase fault event [18]. However, the post-fault operation substantially increases the injected current in healthy winding sets for a given torque level [5], [18].

The comparison between the torque computed from the flux maps in faulty conditions and the measured torque using the transducer for each test point of the identification procedure is shown in Fig. 13.

It is noted how the two values match each other for all test points of the identification procedure, validating the results obtained by the latter also in severe open-three-phase fault conditions.

V. Conclusion

This paper proposed a test procedure to directly identify flux and torque maps of a multi-three-phase synchronous motor presenting an arbitrary number of three-phase winding sets and generic rotor structure with anisotropy and permanent magnets (PMs). No constraints exist on the stator winding configuration that can also differ from those symmetrical or asymmetrical. Besides, the proposed test procedure can straightforwardly identify flux and torque maps of the motor under test also in severe open-three-phase fault conditions, i.e., loss of one or more three-phase units, still getting accurate results.

Experimental results obtained on a 12-phase PM-assisted synchronous reluctance motor adopting a quadruple-three-phase stator winding configuration validate the proposed identification procedure in healthy and open-three-phase fault conditions (loss of two three-phase units over the rated four).

Acknowledgment

The authors would like to acknowledge the financial support from the Power Electronic Innovation Center (PEIC) of Politecnico di Torino (www.peic.polito.it).

References

[1] R. Bojoi, S. Rubino, A. Tenconi, and S. Vaschetto, 'Multiphase electrical machines and drives: A viable solution for energy generation and transportation electrification', in *2016 International Conference and Exposition on Electrical and Power Engineering (EPE)*, Oct. 2016, pp. 632–639. doi: 10.1109/ICEPE.2016.7781416.

[2] W. Cao, B *et al.*, 'Overview of Electric Motor Technologies Used for More Electric Aircraft (MEA)', *IEEE Trans. Ind. Electron.*, vol. 59, no. 9, pp. 3523–3531, Sep. 2012, doi: 10.1109/TIE.2011.2165453.

[3] E. Levi, 'Multiphase Electric Machines for Variable-Speed Applications', *IEEE Trans. Ind. Electron.*, vol. 55, no. 5, pp. 1893–1909, May 2008, doi: 10.1109/TIE.2008.918488.

[4] S. Rubino, I. R. Bojoi, F. Mandrile, and E. Armando, 'Modular Stator Flux and Torque Control of Multi-Three-Phase Induction Motor Drives', *IEEE Trans. Ind. Appl.*, vol. 56, no. 6, pp. 6507–6525, Nov. 2020, doi: 10.1109/TIA.2020.3022338.

[5] S. Rubino, O. Dordevic, R. Bojoi, and E. Levi, 'Modular Vector Control of Multi-Three-Phase Permanent Magnet Synchronous Motors', *IEEE Trans. Ind. Electron.*, vol. 68, no. 10, pp. 9136–9147, Oct. 2021, doi: 10.1109/TIE.2020.3026271.

[6] I. Zoric, M. Jones, and E. Levi, 'Arbitrary Power Sharing Among Three-Phase Winding Sets of Multiphase Machines', *IEEE Trans. Ind. Electron.*, vol. 65, no. 2, pp. 1128–1139, Feb. 2018, doi: 10.1109/TIE.2017.2733468.

[7] D. Cittanti *et al.*, 'Analysis and Design of a High Power Density Full-Ceramic 900 V DC-Link Capacitor for a 550 kVA Electric Vehicle Drive Inverter', in *2022 International Power Electronics Conference (IPEC-Himeji 2022- ECCE Asia)*, May 2022, pp. 1144–1151. doi: 10.23919/IPEC-Himeji2022-ECCE53331.2022.9807220.

[8] F. Stella, G. Pellegrino, E. Armando, and D. Daprà, 'Advanced testing of SiC power MOSFET modules for electric motor drives', in *2017 IEEE International Electric Machines and Drives Conference (IEMDC)*, May 2017, pp. 1–8. doi: 10.1109/IEMDC.2017.8002314.

[9] F. Stella, G. Pellegrino, and E. Armando, 'Three-phase SiC inverter with active limitation of all MOSFETs junction temperature', *Microelectron. Reliab.*, vol. 110, p. 113659, Jul. 2020, doi: 10.1016/j.microrel.2020.113659.

[10] N. Bianchi, J. Park, A. Tortella, and R. Zavagnin, 'Experimental Tests of Dual Three-Phase Synchronous Reluctance Motor Under Half-Control Mode', *IEEE Trans. Ind. Appl.*, vol. 57, no. 6, pp. 5887–5893, Nov. 2021, doi: 10.1109/TIA.2021.3108745.

[11] L. Alberti and N. Bianchi, 'Experimental Tests of Dual Three-Phase Induction Motor Under Faulty Operating Condition', *IEEE Trans. Ind. Electron.*, vol. 59, no. 5, pp. 2041–2048, May 2012, doi: 10.1109/TIE.2011.2171175.

[12] M. Slunjski, O. Dordevic, M. Jones, and E. Levi, 'Symmetrical/Asymmetrical Winding Reconfiguration in Multiphase Machines', *IEEE Access*, vol. 8, pp. 12835–12844, 2020, doi: 10.1109/ACCESS.2020.2965652.

[13] I. Zoric, M. Jones, and E. Levi, 'Vector space decomposition algorithm for asymmetrical multiphase machines', in *2017 International Symposium on Power Electronics (Ee)*, Oct. 2017, pp. 1–6. doi: 10.1109/PEE.2017.8171682.

[14] I. R. Bojoi, E. Armando, G. Pellegrino, and S. G. Rosu, 'Self-commissioning of inverter nonlinear effects in AC drives', in *2012 IEEE International Energy Conference and Exhibition (ENERGYCON)*, Sep. 2012, pp. 213–218. doi: 10.1109/EnergyCon.2012.6347755.

[15] Y. Zhao and T. A. Lipo, 'Space vector PWM control of dual three-phase induction machine using vector space decomposition', *IEEE Trans. Ind. Appl.*, vol. 31, no. 5, pp. 1100–1109, Sep. 1995, doi: 10.1109/28.464525.

[16] R. H. Nelson and P. C. Krause, 'Induction Machine Analysis for Arbitrary Displacement Between Multiple Winding Sets', *IEEE Trans. Power Appar. Syst.*, vol. PAS-93, no. 3, pp. 841–848, May 1974, doi: 10.1109/TPAS.1974.293983.

[17] S. Rubino, F. Mandrile, E. Armando, I. R. Bojoi, and L. Zarri, 'Fault-Tolerant Torque Controller Based on Adaptive Decoupled Multi-Stator Modeling for Multi-Three-Phase Induction Motor Drives', *IEEE Trans. Ind. Appl.*, vol. 58, no. 6, pp. 7318–7335, Nov. 2022, doi: 10.1109/TIA.2022.3197547.

[18] S. Rubino, O. Dordevic, E. Armando, I. R. Bojoi, and E. Levi, 'A Novel Matrix Transformation for Decoupled Control of Modular Multiphase PMSM Drives', *IEEE Trans. Power Electron.*, vol. 36, no. 7, pp. 8088–8101, Jul. 2021, doi: 10.1109/TPEL.2020.3043083.

[19] S. Rubino, R. Bojoi, D. Cittanti, and L. Zarri, 'Decoupled and Modular Torque Control of Multi-Three-Phase Induction Motor Drives', *IEEE Trans. Ind. Appl.*, vol. 56, no. 4, pp. 3831–3845, 2020, doi: 10.1109/TIA.2020.2991122.

[20] S.-K. Sul, *Control of Electric Machine Drive Systems*. in IEEE Press Series on Power Engineering. New York, NY: John Wiley & Sons, 2011.

[21] B. Stumberger, G. Stumberger, D. Dolinar, A. Hamler, and M. Trlep, 'Evaluation of saturation and cross-magnetization effects in interior permanent-magnet synchronous motor', *IEEE Trans. Ind. Appl.*, vol. 39, no. 5, pp. 1264–1271, Sep. 2003, doi: 10.1109/TIA.2003.816538.

[22] E. Armando, R. I. Bojoi, P. Guglielmi, G. Pellegrino, and M. Pastorelli, 'Experimental Identification of the Magnetic Model of Synchronous Machines', *IEEE Trans. Ind. Appl.*, vol. 49, no. 5, pp. 2116–2125, Sep. 2013, doi: 10.1109/TIA.2013.2258876.

[23] F. Stella, A. Yousefi-Talouki, S. Odhano, G. Pellegrino, and P. Zanchetta, 'An Accurate Self-Commissioning Technique for Matrix Converters Applied to Sensorless Control of Synchronous Reluctance Motor Drives', *IEEE J. Emerg. Sel. Top. Power Electron.*, vol. 7, no. 2, pp. 1342–1351, Jun. 2019, doi: 10.1109/JESTPE.2018.2851142.

[24] A. Yousefi-Talouki *et al.*, 'Sensorless control of matrix converter-fed synchronous reluctance motor drives', in *2017 IEEE International Symposium on Sensorless Control for Electrical Drives (SLED)*, Sep. 2017, pp. 181–186. doi: 10.1109/SLED.2017.8078421.

[25] E. Armando, P. Guglielmi, G. Pellegrino, and R. Bojoi, 'Flux linkage maps identification of synchronous AC motors under controlled thermal conditions', in *2017 IEEE International Electric Machines and Drives Conference (IEMDC)*, May 2017, pp. 1–8. doi: 10.1109/IEMDC.2017.8002334.

[26] F. Mariut, S. Rosu, R. Bojoi, and A. Tenconi, 'Multiphase modular power converter using the PEBB concept and FPGA-based direct high speed voltage measurement', in *2015 17th European Conference on Power Electronics and Applications (EPE'15 ECCE-Europe)*, Sep. 2015, pp. 1–10. doi: 10.1109/EPE.2015.7309332.

[27] E. Armando, P. Guglielmi, G. Pellegrino, M. Pastorelli, and A. Vagati, 'Accurate Modeling and Performance Analysis of IPM-PMASR Motors', *IEEE Trans. Ind. Appl.*, vol. 45, no. 1, pp. 123–130, Jan. 2009, doi: 10.1109/TIA.2008.2009493.